Persistent wind-induced enhancement of diffusive CO_2 transport in a mountain forest snowpack

D. R. Bowling[1] and W. J. Massman[2]

Received 29 March 2011; revised 10 June 2011; accepted 13 July 2011; published 20 October 2011.

[1] Diffusion dominates the transport of trace gases between soil and the atmosphere. Pressure gradients induced by atmospheric flow and wind interacting with topographical features cause a small but persistent bulk flow of air within soil or snow. This forcing, called pressure pumping or wind pumping, leads to a poorly quantified enhancement of gas transport beyond the rate of molecular diffusion. This study was conducted to quantify the role of pressure pumping in enhancement of CO_2 transport through a mountain forest seasonal snowpack. Observations of $^{12}CO_2$ and $^{13}CO_2$ within the snowpack, soil, and air of a subalpine forest were made over three winters in the Rocky Mountains, USA. These molecules differ in their rates of diffusion, providing a means to quantify the relative importance of diffusion and advection. An empirical model was developed to describe the transport of these gases through the snowpack, assuming that isotopic variability was caused solely by wind. We found that advection was a persistent phenomenon within the snowpack. Under calm conditions, isotopic patterns followed those associated with diffusion. In the presence of wind, the 4.4‰ isotopic effect of diffusion was diminished, and transport was enhanced beyond the diffusive rate for a given mole fraction gradient. Pressure pumping in our forest snowpack enhanced transport of CO_2 beyond molecular diffusion by up to 40% in the short term (hours) but by at most 8%–11% when integrated over a winter. These results should be applicable to trace gas transport in a variety of biogeochemical applications.

Citation: Bowling, D. R., and W. J. Massman (2011), Persistent wind-induced enhancement of diffusive CO_2 transport in a mountain forest snowpack, *J. Geophys. Res.*, *116*, G04006, doi:10.1029/2011JG001722.

1. Introduction

[2] A thorough understanding of the different mechanisms of gas transport through snow is required for investigation of many winter biogeochemical processes. A variety of gases move through the snowpack, including those produced or consumed by microbial, plant, and animal activity, and biologically inert gases transported (in either direction) between geochemical and atmospheric reservoirs [e.g., *Helmig et al.*, 2009]. Cold-season biological activity produces gases that are both ecologically and radiatively important, including CO_2, CH_4, and N_2O [*Massman et al.*, 1997; *Sommerfeld et al.*, 1993]. Under-snow production of these gases can amount to a significant component of their annual biosphere–atmosphere exchange [*Groffman et al.*, 2006; *Liptzin et al.*, 2009], and can be amplified by physical processes such as onset of freezing in early winter or freeze-thaw events [*Elberling and Brandt*, 2003; *Mastepanov et al.*, 2008; *Wu et al.*, 2010], particularly when the snowpack is shallow.

[3] Several methods have been used to monitor trace gas transport through snow, including chambers on the snow surface [*Groffman et al.*, 2006] or the soil surface following snow removal [*Elberling and Brandt*, 2003], observations of trace gas gradients within [*Sommerfeld et al.*, 1993] or above the snow [*Honrath et al.*, 2002], eddy covariance [*Lafleur et al.*, 2001], tracer release [*Albert and Shultz*, 2002], and stable isotope mixing profiles [in firn, *Kawamura et al.*, 2006]. When methods are compared, they sometimes provide quite different estimates of trace gas flux [*Björkman et al.*, 2010; *McDowell et al.*, 2000]. The most common is probably the within-snow gradient method, which is almost always applied assuming transport by molecular diffusion alone. However, we have known for some time that wind affects trace gases in snow and soils [*Kelley et al.*, 1968; *Kimball and Lemon*, 1970, 1971a, 1971b], and there is increasing recognition of the importance of nondiffusive transport within snow [*Massman et al.*, 1997; *Sommerfeld et al.*, 1996; *Takagi et al.*, 2005] and soils [*Fujiyoshi et al.*, 2010; *Lewicki et al.*, 2010; *Maier et al.*, 2010]. Empirical studies are needed to quantify the influence of pressure pumping on biogeochemical trace gases in porous media.

[4] In the absence of bulk airflow, gases are transported by molecular diffusion along gradients of mole fraction. Under calm conditions, gases produced in the soil diffuse through

[1]Department of Biology, University of Utah, Salt Lake City, Utah, USA.
[2]Rocky Mountain Research Station, USDA Forest Service, Fort Collins, Colorado, USA.

0148-0227/11/2011JG001722

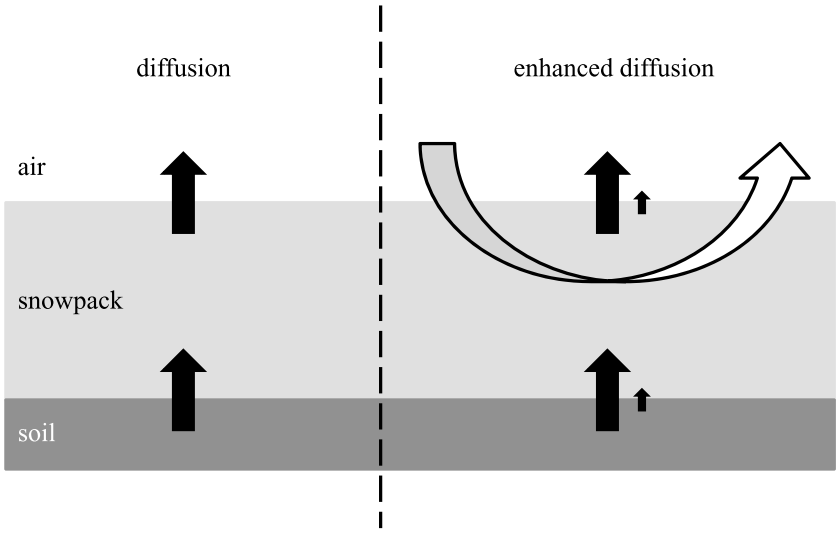

Figure 1. Conceptual diagram of the enhancement of diffusion caused by wind-induced snowpack ventilation, illustrating (left) a non-windy case in which the diffusive soil respiration flux (designated by the arrow) enters and leaves the snowpack and (right) how ventilation of the snowpack by pressure pumping can lead to an enhancement of flux rate (small arrow) beyond that due to molecular diffusion alone (large arrow) for a given gradient in CO_2. Note that the actual CO_2 production rate by respiration is not changed, but the transport is enhanced.

the snowpack and out to the atmosphere (Figure 1, left). Pressure changes caused by large-scale atmospheric dynamics such as synoptic fronts and gravity waves, and by wind interacting with local-scale topographical features, lead to bulk airflow within porous media [see *Massman*, 2006, citations]. Collectively this forcing has been called pressure pumping or wind pumping [*Clarke and Waddington*, 1991; *Colbeck*, 1989; *Massman et al.*, 1997]. The depth to which bulk airflow penetrates into a snowpack with pressure pumping is difficult to assess because the air velocity cannot be directly measured. Bulk flow caused by wind shear is limited to the top millimeters to centimeters of the snow [*Clifton et al.*, 2008], but effects on trace gases can penetrate fully through a 2 m seasonal snowpack [*Seok et al.*, 2009] and to tens of meters within firn [*Kawamura et al.*, 2006]. The effect is easily observed in temperature gradients within snow while a fan blows across the surface of the snow [*Albert and Hardy*, 1995]. Although convection is probably rare, temperature gradients can induce airflow in the snowpack, especially horizontally [*Sturm and Johnson*, 1991]. Such gradients may result from pressure pumping, or from unrelated spatial heterogeneity in energy balance.

[5] Air moving within the snowpack enhances the transport of gases through advection and dispersion. However, bulk air velocities within snow and firn are on the order of 10^{-3} to 10^{-2} m s^{-1} [*Albert and Hawley*, 2002; *Albert and Shultz*, 2002; *Sokratov and Sato*, 2000] and even smaller in soils [*Camarda et al.*, 2007]. Hence the transport of gases by bulk flow is likely smaller than by molecular diffusion. The net effect of pressure pumping is to provide an enhancement to transport that would otherwise occur by diffusion alone (Figure 1, right). Note that pressure pumping probably does not enhance biogeochemical *production* of trace gases but instead increases the transport along a given mole fraction gradient beyond the diffusive rate.

[6] Stable isotopes of CO_2 provide information about the relative contributions of diffusion and advection to transport of CO_2 within porous media. The relevant mixing relationships are shown in Figure 2, with measured quantities (the CO_2 mole fraction and its carbon isotope composition, $\delta^{13}C$) in Figure 2a and the $1/CO_2$ variant commonly called a Keeling plot [*Keeling*, 1958] in Figure 2b. The corresponding lines (solid and dashed) of the two panels represent the same two mixing relationships; equations to describe these lines are available elsewhere [see *Bowling et al.*, 2009]. In Figure 2b, CO_2 in air (open circle) mixes with CO_2 produced by respiration (having $\delta^{13}C$ of respiration indicated by the black square) along a straight line between them, but only under conditions where bulk fluid flow dominates over diffusion. In this situation, such as would occur in a turbulent forest atmosphere, air resulting from the mixing would be observed along the advection-dominated line [*Pataki et al.*, 2003]. By contrast, if the mixing occurs by diffusion only, the resulting air will follow the diffusion-only line. The intercepts of the lines in Figure 2b are separated by 4.4‰ due to a mass-dependent isotopic fractionation caused by the difference in the binary diffusivities of $^{12}CO_2$ and $^{13}CO_2$ in air [*Cerling et al.*, 1991]. In a porous medium where diffusion and advection both contribute to gas transport, such as the snowpack or soil, the resulting air will be found in the enhanced-diffusion zone between the two lines [*Bowling et al.*, 2009].

[7] Short-term changes in CO_2 gradients and associated isotope effects are caused by wind-induced ventilation of the snowpack, an effect that has been reported in many studies [*Maier et al.*, 2010; *Massman and Frank*, 2006; *Seok et al.*, 2009; *Takagi et al.*, 2005]. During such events, the mole fraction gradient and the temporal change in CO_2 stored within the snowpack can be used to quantify the CO_2 fluxes from the snowpack (we will formalize these fluxes below). However, the diffusive flux and change in storage

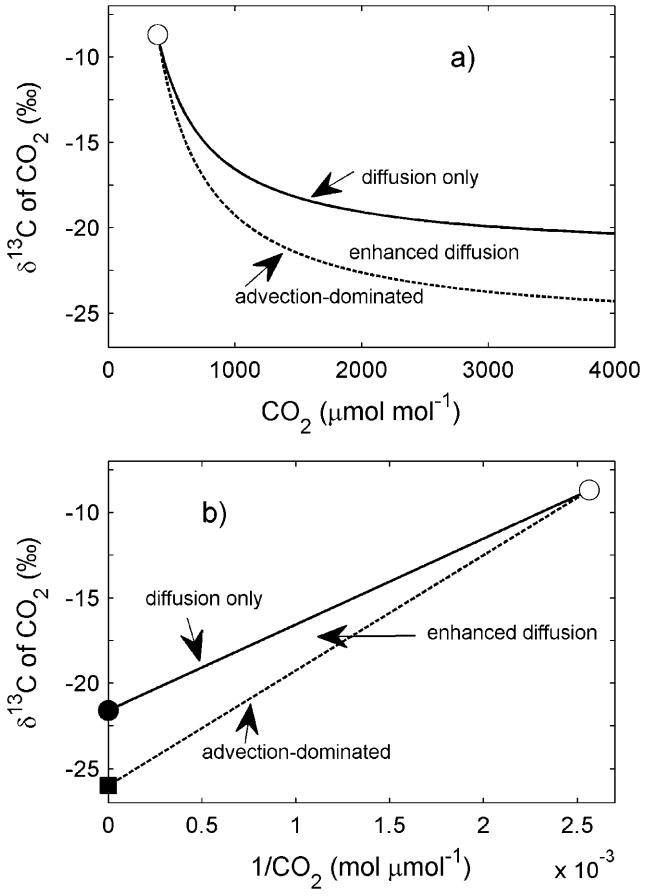

Figure 2. Theoretical mixing relationships of CO_2 and $\delta^{13}C$ of CO_2 when air mixes with soil-respired CO_2, with (a) the measured quantities and (b) the Keeling-plot version shown. The lines represent the same mixing relationships in both panels. Under nondiffusive conditions, the air outside the snowpack (open circle) will mix along the dashed line with CO_2 produced by respiration (with $\delta^{13}C$ indicated by the square). Under fully diffusive conditions, a kinetic fractionation affects the CO_2 within the snowpack, and mixing follows the solid line. The y-intercepts of the lines in Figure 2b are separated by 4.4‰, and a Keeling plot constructed with samples collected under fully diffusive conditions will have an intercept (solid circle) that is more enriched than the actual respiratory source (square). The zone in between represents the variable isotopic effect associated with enhanced diffusion. For this figure an assumed $\delta^{13}C$ of respiration of −26‰ was used [*Bowling et al.*, 2009].

do not fully account for the transport induced by pressure pumping. As we will show, wind leads to an enhancement of transport for a given trace gas gradient beyond that associated with molecular diffusion, because it leads to a small but persistent flow of bulk air within the snowpack.

[8] In this study, we report an experiment designed to quantify the role of pressure pumping in enhancement of CO_2 transport through a mountain forest seasonal snowpack. CO_2 and its isotopic composition were monitored for three winters within the snowpack, soil, and air of a subalpine forest in the southern Rocky Mountains of Colorado, USA. We assume that variation in CO_2 isotope mixing within a snowpack can be attributed solely to the influence of wind on gas transport, and we use CO_2 isotopic variation as a metric for transport enhancement. We first develop a model to quantify the pressure pumping effect on gas transport, and then provide a detailed description of the experimental observations, their application, and our results.

2. Snowpack Gas Transport Model

[9] Transport of gases is governed by mass conservation in three spatial dimensions. Here we simplify to one, and assume a two-layer medium consisting of the soil (which produces CO_2 via biological respiration) and the snowpack (which we assume does not produce or consume CO_2). The diffusive flux of $^{12}CO_2$ leaving the snowpack (^{12}F) under steady state conditions can be represented in the vertical (z) dimension using Fick's first law of diffusion

$$^{12}F = -\rho_a \eta \tau\, ^{12}D \frac{d^{12}C}{dz}, \tag{1}$$

where ρ_a is the molar density of air (adjusted for temperature and pressure using the Boyle-Charles law), η and τ are the air-filled porosity and tortuosity of the snowpack, respectively, ^{12}D is the molecular diffusivity of $^{12}CO_2$ in air (adjusted for temperature and pressure following *Massman* [1998]), and ^{12}C the mole fraction of $^{12}CO_2$ at height z. (A list of symbols is provided in Table 1.) We assume ρ_a and η are independent of location in the snowpack. A similar equation applies to the heavy isotopologue

$$^{13}F = -\rho_a \eta \tau\, ^{13}D \frac{d^{13}C}{dz}, \tag{2}$$

where the molecular diffusivity of $^{13}CO_2$ in air (^{13}D) is given by *Cerling et al.* [1991]:

$$\frac{^{12}D}{^{13}D} = 1.0044. \tag{3}$$

When equation (1) is applied at discrete time intervals, there may be a change in the mole fraction of either isotopologue, in which case the height-integrated rate of change of CO_2 stored in the snowpack must be accounted for. We will refer to this as the storage flux, defined by

$$^{12}F_s = -\rho_a \eta \int_{z_1}^{z_2} \frac{d^{12}C}{dt} dz, \tag{4}$$

where z_1 and z_2 are the relevant heights within the snowpack (typically the bottom and top of the snowpack, but the litter and mineral soil might also be included). A similar equation applies for $^{13}CO_2$. The total flux of $^{12}CO_2$ or $^{13}CO_2$ produced by respiration sources below the snowpack (^{12}S or ^{13}S, respectively) is the sum of the diffusive flux, the storage flux, and additional transport related to advection and dispersion, which are described in full by the mass conservation equation [*Bottacin-Busolin and Marion*, 2010; *Massman*, 2006]. We use the following simpler formulation,

$$^{12}S = ^{12}F + ^{12}F_s + \text{other transport} \tag{5}$$

$$^{13}S = ^{13}F + ^{13}F_s + \text{other transport} \tag{6}$$

Table 1. List of Symbols

Symbol	Units	Description
a	s m^{-1}	linear regression slope (equation (10))
b	dimensionless	linear regression intercept (equation (10))
C	μmol CO_2 mol^{-1}	mole fraction of CO_2 (total)
^{12}C	μmol $^{12}CO_2$ mol^{-1}	mole fraction of $^{12}CO_2$
^{13}C	μmol $^{13}CO_2$ mol^{-1}	mole fraction of $^{13}CO_2$
^{12}D	m^2 s^{-1}	molecular diffusivity of $^{12}CO_2$ in air
^{13}D	m^2 s^{-1}	molecular diffusivity of $^{13}CO_2$ in air
δ	dimensionless (‰)	isotope ratio $^{13}C/^{12}C$ in delta notation ($\delta^{13}C$)
δ_a, δ_b	dimensionless (‰)	isotope ratio $^{13}C/^{12}C$ of individual CO_2 sources mixing (equation (14))
δ_s	dimensionless (‰)	isotope ratio $^{13}C/^{12}C$ of source (respiratory production) flux
η	dimensionless	air-filled porosity of the snowpack
F_a, F_b	μmol CO_2 m^{-2} s^{-1}	flux of individual CO_2 sources mixing (equation (14))
^{12}F	μmol $^{12}CO_2$ m^{-2} s^{-1}	diffusive flux of $^{12}CO_2$ leaving the snowpack (equation (1))
^{13}F	μmol $^{13}CO_2$ m^{-2} s^{-1}	diffusive flux of $^{13}CO_2$ leaving the snowpack (equation (2))
$^{12}F_{enh}$	μmol $^{12}CO_2$ m^{-2} s^{-1}	enhanced flux of $^{12}CO_2$ leaving the snowpack (equation (12))
$^{13}F_{enh}$	μmol $^{13}CO_2$ m^{-2} s^{-1}	enhanced flux of $^{13}CO_2$ leaving the snowpack (equation (13))
$^{12}F_s$	μmol $^{12}CO_2$ m^{-2} s^{-1}	storage flux of $^{12}CO_2$
$^{13}F_s$	μmol $^{13}CO_2$ m^{-2} s^{-1}	storage flux of $^{13}CO_2$
i	dimensionless	finite difference index
K	m^2 s^{-1}	enhanced diffusivity of CO_2 in air (same for $^{12}CO_2$ and $^{13}CO_2$)
n	dimensionless	number of samples
p	dimensionless	probability of significant relationship
r^2	dimensionless	coefficient of determination of linear regression
R_{VPDB}	dimensionless	$^{13}C/^{12}C$ ratio of Vienna PDB isotope standard
ρ_a	mol m^{-3}	molar density of air
ρ_{snow}	kg m^{-3}	density of snow
ρ_{ice}	kg m^{-3}	density of ice
^{12}S	μmol $^{12}CO_2$ m^{-2} s^{-1}	source (respiratory production) flux of $^{12}CO_2$ per unit area
^{13}S	μmol $^{13}CO_2$ m^{-2} s^{-1}	source (respiratory production) flux of $^{13}CO_2$ per unit area
SWE	mm	snow water equivalent
t	sec	time
τ	dimensionless	tortuosity of the snowpack
U	m s^{-1}	horizontal wind speed above the forest canopy
z	m	height relative to ground

which allows us to bulk the nondiffusive effects into a wind-dependent enhanced diffusivity. Taking the ratio of equations (6) and (5), and expanding the diffusivity terms to include both a molecular and an enhanced diffusivity (**K**), we obtain

$$\frac{^{13}S}{^{12}S} = \frac{-\rho_a \eta \tau (^{13}D + K)\dfrac{d^{13}C}{dz} + {}^{13}F_s}{-\rho_a \eta \tau (^{12}D + K)\dfrac{d^{12}C}{dz} + {}^{12}F_s} \tag{7}$$

In this formulation, we have eliminated the bulk flow terms, and have instead accounted for them using **K**, which allows a Fick's law framework to be used. Since the additional transport is forced by bulk fluid flow (advection/dispersion), the enhanced diffusivity is independent of mass and is the same for both isotopologues. The ratio of the source fluxes ($^{13}S/^{12}S$) is the same conceptually as the isotope ratio of the total respiration flux, which is expressed in the usual fashion:

$$\delta_S = \left(\frac{^{13}S/^{12}S}{R_{VPDB}} - 1\right) \times 1000. \tag{8}$$

Equation (7) can be rearranged to solve for **K**:

$$K = \frac{(^{13}F + {}^{13}F_s) - \dfrac{^{13}S}{^{12}S}(^{12}F + {}^{12}F_s)}{-\rho_a \eta \tau \left(\dfrac{^{13}S}{^{12}S}\dfrac{d^{12}C}{dz} - \dfrac{d^{13}C}{dz}\right)} \tag{9}$$

[10] Here we assume the isotopic composition of the soil respiration flux (δ_S, and hence $^{13}S/^{12}S$) is constant (this will be discussed further later). Under this condition, departure from the strict diffusive mixing case can only be caused by wind-induced ventilation of the snowpack and soil (Figure 2). If δ_S is constant and isotopic mixing processes (quantified by the terms on the right-hand side of equation (9)) depart from the diffusive case, we can quantify the influence of the wind on transport. Under these conditions **K** in equation (9) will be a function of a fluid transport forcing parameter such as wind speed or pressure.

[11] Pressure effects related to enhanced diffusivity have been assumed (or observed) to be a function of wind velocity (U) to the first or second power, or exponentially [*Colbeck*, 1989; *Massman and Frank*, 2006; *Seok et al.*, 2009; *Waddington et al.*, 1996]. We initially attempted to use equation (9) to relate **K** to U and U^2 but were sometimes confronted with small differences and mathematical instability. A more stable variant can be expressed as

$$\frac{(^{12}D + K)}{(^{13}D + K)} = aU + \mathbf{b}. \tag{10}$$

The term on the left is the ratio of the total diffusivity (molecular diffusivity + enhanced diffusivity) of $^{12}CO_2$ (numerator) to that for $^{13}CO_2$ (denominator). Under perfectly calm conditions (U = 0), transport is by diffusion only, with no wind-enhancement of transport (**K** = 0), and equation (10) converges to equation (3). Thus, a regression of (^{12}D + **K**)/(^{13}D + **K**) versus U, where **K** is calculated using equation (9), should have an intercept b = 1.0044. When wind does enhance the rate of diffusion, differences between the rates of diffusion for the two isotopologues will be decreased compared to the molecular diffusivity ratio (equation (3)); so the slope a should always be negative.

[12] Finally, we define an enhancement factor to illustrate the magnitude of the wind effect on transport relative to diffusion. In general, the diffusive enhancement factor is the ratio of a nondiffusive flux to a diffusive flux, in our case expressed by the ratio **K**/^{12}D. When there is no wind enhancement (**K** = 0), the enhancement factor **K**/^{12}D = 0, and when wind increases the total flux relative to the strictly diffusive case, then **K**/^{12}D > 0. As we will show, values for **K**/^{12}D are typically 0.0 to 0.4, implying that pressure pumping

within our temperate snowpack can enhance transport by up to 40% beyond molecular diffusion for a given mole fraction gradient.

3. Methods

3.1. Study Location

[13] This work was conducted in a Colorado subalpine forest (the Niwot Ridge AmeriFlux site, 40.03°N, 105.55°W, 3050 m elevation). The roughly 110-year-old forest is dominated by three conifers, *Pinus contorta*, *Picea engelmannii*, and *Abies lasiocarpa*. The forest is on a glacial moraine with a slope of about 6°–7°. The vegetation canopy is 11–12 m tall, with a leaf area index of 3.8–4.2 m^2 m^{-2}, a zero-plane displacement height of 7.6 m, and a roughness length of 1.8 m [*Turnipseed et al.*, 2002]. Mean annual temperature is 1.5°C, and mean annual precipitation is 800 mm. Average peak snow water equivalent (SWE) is 328 mm on 21 April (Natural Resources Conservation Service, http://www.wcc.nrcs.usda.gov/snotel/, 1971–2000). Snow cover at the site generally lasts from October/November through May/June. Further site details are available elsewhere [*Hu et al.*, 2010; *Monson et al.*, 2002]. Field research was conducted during three consecutive winters, which will be referred to as W1 (winter 1, 2006/2007), W2 (winter 2, 2007/2008), and W3 (winter 3, 2008/2009).

3.2. CO_2 and CO_2 Isotopes Within the Snowpack

[14] Vertical profiles of $^{12}CO_2$ and $^{13}CO_2$ mole fractions within the snowpack and soil were monitored using tunable diode laser absorption spectrometry as detailed by Bowling *et al.* [2009]. These were used separately in the equations above and also converted to CO_2 (their sum) and $\delta^{13}C$ of CO_2 (their ratio). Although multiple profiles were measured in W1, data are presented in this paper from a single forest location [*Bowling et al.*, 2009, profile 2], which was continuously used all 3 years. Measurement heights differed for the profile each winter, but the forest location was identical. During W1, measurement heights were −5 cm (within the O-horizon), 0 (litter–snow interface), 20, 40, 60, 80, 100, 120, and 200 cm (the higher inlets were sometimes or always in the air and not the snowpack). During both W2 and W3, inlets were at −5, 0, 30, 60, and 200 cm, with the addition of a deep mineral soil (−35 cm) measurement in W3. There were three inlet locations common to all three winters (−5, 0, and 200 cm). During W1, observations began in February and lasted through snowmelt, during W2 and W3, they lasted for the full winter from first snow to snowmelt. The inlet sampling lines flowed only when sampling, which disrupted a sphere of radius <7 cm at the inlet. We estimate that the gradient was re-established within 10 min of sampling (details provided in [*Bowling et al.*, 2009]). A full profile was always measured within a 30 min period, and this cycle was repeated every 3 h.

3.3. Wind, Soil Moisture, and Snowpack

[15] Wind velocity data measured at 21.5 m (roughly 10 m above the canopy) were obtained from the ongoing Niwot Ridge AmeriFlux tower measurement program [*Monson et al.*, 2002]. In addition, soil moisture was measured at three surface locations within 1–5 m horizontally from the gas inlets, using water content reflectometers at 0–10 cm depth (CS616, Campbell Scientific, Inc., Logan, Utah).

[16] The physical characteristics of the snowpack were determined by direct measurement in hand-excavated pits. Pits were sampled roughly every 10 days at representative locations within 10 m of the gas inlets, following *Williams et al.* [1999]. Measurements included density, SWE (every 10 cm vertically), and total snow depth. The number of pits sampled each winter varied (11, 16, and 21 pits in W1, W2, and W3, respectively). SWE (determined with a snow pillow produced by Rickly Hydrological Company, Columbus, Ohio) and snow depth (measured with an ultrasonic depth sensor produced by Judd Communications, Salt Lake City, Utah) were monitored continuously, at a similar location, slope, and aspect ~400 m from the gas inlets by the USDA/NRCS Snow Survey Program (http://www.wcc.nrcs.usda.gov/snotel/).

3.4. CO_2 Fluxes From the Snowpack

[17] Fluxes were calculated using Fick's law with storage flux (equations (1)–(4)) using three methods (A, B, C, described below), each with an increasing number of measurements and complexity. Method A was used for all winters; methods B and C were used to examine W3 in detail. We did this for W3 only because this period had the most detailed observational coverage of the full snowpack–soil system and provided the best opportunity to assess how our different flux methods might influence conclusions about pressure pumping.

[18] For all methods, the nearest above-snow inlet was taken to be representative of the air just above the actual snow surface. To calculate the storage flux (equation (4)) using subsequent discrete sampling times, a centered finite difference method was used to estimate the derivative dC/dt at the time when the mole fraction gradients were measured. For this,

$$\frac{dC}{dt}(i) = \frac{c(i+1) - c(i-1)}{2\Delta t}, \tag{11}$$

where i is the time interval when the diffusive and storage fluxes are calculated, $i-1$ and $i+1$ are the times 3 h before and after i, and Δt is the time difference between subsequent samples (3 h).

3.4.1. Method A (The Simple Method)

[19] Two measurement inlets (0 and 200 cm, 30 and 200 cm, or 60 and 200 cm, depending on the analysis) were used to calculate the mole fraction gradients across the snowpack ($d^{12}C/dz$ and $d^{13}C/dz$). The storage fluxes in the snowpack were calculated using the mean dC/dt calculated at the two inlets and equation (4). Storage fluxes in the litter and soil were ignored.

3.4.2. Method B (The Intensive Measurement Method)

[20] All measurement inlets were used to calculate a mean gradient across the snowpack (a linear regression of C versus z through all snowpack inlets), and the storage flux was calculated in each layer between successive measurement inlets. Litter and soil storage were calculated assuming a litter layer between −5 and 0 cm, and a mineral soil layer between −35 and −5 cm. Air-filled porosity for each soil layer was calculated using measured soil water content and bulk density for each layer [*Scott-Denton et al.*, 2003].

3.4.3. Method C (The Measurement/Modeling Method)

[21] This was similar to method B, but an empirical fit was added to create continuous mole fraction profiles through the

Table 2. Relations Between Snowpack Physical Characteristics Measured in Hand-Excavated Pits (Roughly Weekly) and Those Continuously Measured at the SNOTEL Site[a]

Pit Depth Versus SNOTEL Depth					
Time Period	Slope	Intercept	r^2	n	p
All winters	0.790	11.04	0.646	48	<0.001
W1	0.416	59.32	0.317	11	0.070
W2	0.599	30.08	0.406	16	0.008
W3	0.724	10.07	0.725	21	<0.001
Mean Pit Density Versus SNOTEL Density					
Time Period	Slope	Intercept	r^2	n	p
All winters	0.780	84.81	0.642	48	<0.001
W1	0.450	180.3	0.378	11	0.040
W2	0.994	47.98	0.726	16	<0.001
W3	0.933	33.59	0.820	21	<0.001

[a]Linear regression results are shown for all three winters combined or for each winter separately.

snowpack and soil. Measured profiles were interpolated to 1 cm resolution using a piecewise cubic Hermite interpolation (Matlab 7.9.0 R2009b, The Mathworks, Natick, Massachusetts). A mean gradient across the snowpack was calculated by regression of C versus z through all 1 cm layers within the snowpack. Litter storage was calculated by summing the mean storage in 1 cm layers between −5 and 0 cm. Soil storage was calculated similarly (−75 to −5 cm). The deepest measurement inlet was −35 cm, and this measured value was assigned at −50 cm prior to interpolation of the mole fraction profile, forcing a no-flux boundary at the bottom of the soil. Porosity was calculated as in method B.

[22] For all calculations of flux, we used a bulk characterization of the physical attributes of the snowpack (detailed density profile information are also presented). Physical characteristics influence the flux calculations (equations (1)–(4)) via porosity (η) and toruosity (τ). Porosity of the snowpack was calculated as $\eta = 1 - \frac{\rho_{snow}}{\rho_{ice}}$, where ρ_{snow} is the mean density of the snowpack and ρ_{ice} is the density of ice. Detailed information regarding the vertical profile of ρ_{snow} was only available at discrete intervals (roughly every 10 days, when snow pits were sampled). New snowfall has an influence on snow density and snowpack CO_2, so time resolution better than the snow pit sampling provided was required for calculating fluxes. The depth and density of snow pits within 10 m of the gas measurements compared favorably to the SNOTEL site 400 m away (Table 2). Since the latter were available on a daily basis, these were used to calculate snow depth and ρ_{snow} on a daily basis, scaled to match snow pit observations when they were available, then interpolated to match our 3 h sampling scheme.

[23] Tortuosity was assumed constant at 0.85, based on detailed measurements made in a similar Rocky Mountain snowpack in southern Wyoming [*Massman et al.*, 1997]. We also allowed τ to vary as a function of porosity [*Hubbard et al.*, 2005; *Monson et al.*, 2006], with negligible difference in results (data not shown).

[24] Total CO_2 fluxes were calculated in two ways, which we refer to as "regular" and "enhanced" fluxes. *Regular fluxes:* Nondiffusive effects were ignored, and total fluxes were calculated using equations (1)–(6), using molecular diffusivity in equations (1)–(2), and including storage fluxes (equation (4) and its ^{13}C variant). *Enhanced fluxes:* The regular fluxes were first used in equations (7)–(10) to assess the dependence of **K** on wind (as described in the next section). Nondiffusive effects were then incorporated into the Fick's law framework by modifying equations (1)–(2) with the wind-dependent enhanced diffusivity **K** as follows

$$ {}^{12}F_{enh} = -\rho_a \eta \tau \left({}^{12}D + K\right) \frac{d^{12}C}{dz} \tag{12} $$

$$ {}^{13}F_{enh} = -\rho_a \eta \tau \left({}^{13}D + K\right) \frac{d^{13}C}{dz} \tag{13} $$

These were added to storage fluxes (which did not differ from the regular flux case) to calculate total enhanced fluxes.

[25] Cumulative fluxes were assessed over each winter, from the time period when measurements began until the snow was gone. This was done with total regular fluxes and total enhanced fluxes, including storage in each case. Missing data were interpolated using a piecewise cubic Hermite interpolation (Matlab 7.9.0 R2009b, The Mathworks, Natick, Massachusetts).

3.5. Dependence of K on Wind

[26] The wind dependence of the enhanced diffusivity was examined using a multistep linear regression and optimization approach. This was done for a variety of cases: combining all winters or examining winters individually, using different selections of inlet heights, and including (or excluding) the storage fluxes. In each case, we assumed a constant value for the isotope ratio of soil respiration (δ_S). This value was unknown but certainly in the range −30‰ to −20‰ [*Bowling et al.*, 2008; *Bowling et al.*, 2009]. Hence we assigned δ_S within this range in steps of 0.1‰, calculated **K** using equation (9) for each, and examined linear regressions (using the fixed δ_S) of diffusivity ratio with above-canopy wind velocity (U) described by equation (10), *without* forcing the intercept b to be 1.0044. Results provided a range of values for the slope and intercept (a and b) over the range examined for δ_S. For each case, we selected the regression that provided an intercept of 1.0044 as the "best" regression since it conformed to theory (equation (10)). Regressions which had the highest correlation (r^2) were generally no better than or only marginally superior to (higher r^2) those where b = 1.0044 (when they differed).

[27] We attempted to use nonlinear multiple regression to simultaneously estimate a, b, and δ_S. Results selected for the best fit regression (minimizing an error metric), which did not necessarily lead to b = 1.0044, violating our expectations based on gas transport theory. We also examined regressions of **K** with U^2. None of these approaches provided any additional physically meaningful insight.

4. Results

[28] In nature the processes of diffusion and advection vary over time in relative importance (e.g., under conditions of pressure pumping induced by variable wind blowing over the snowpack or soil), and CO_2 in the snowpack and soil will be

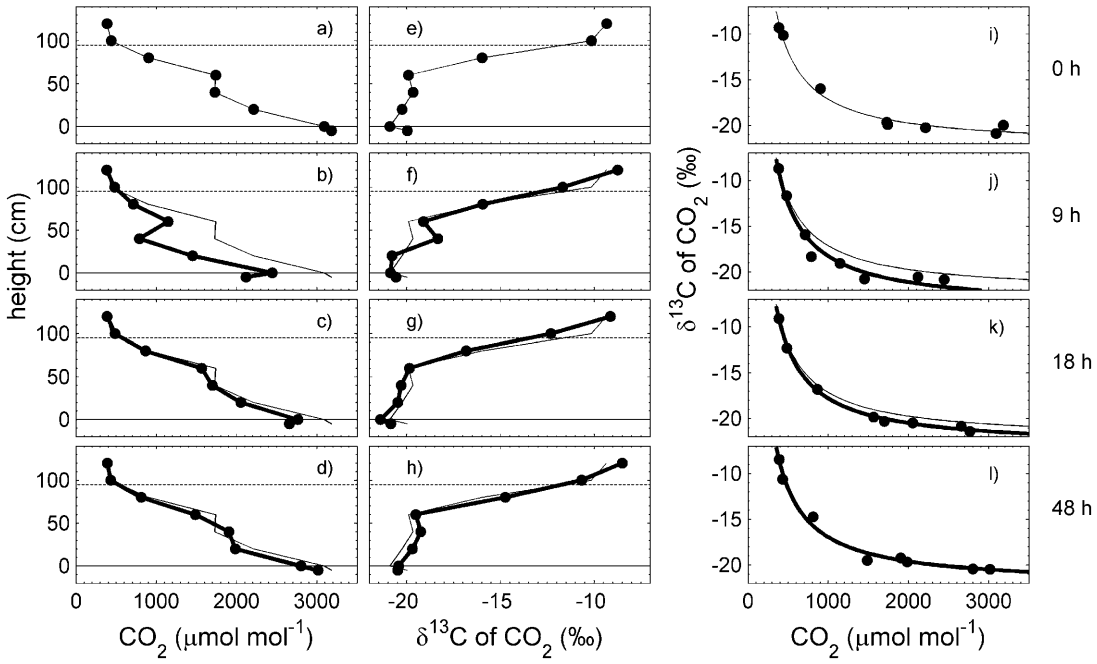

Figure 3. An example of the influence of wind on profiles of (a–d) CO_2 and (e–h) $\delta^{13}C$ of CO_2 within the snowpack and soil. Data are shown from prior to the start of the wind event on 19 April 2007 (Figures 3a, 3e, and 3i) and from 9, 18, and 48 hours later (Figures 3b–3h and 3j–3l). (The wind time series is shown in Figure 9a.) (i–l) The relation between $\delta^{13}C$ and CO_2 at each time period and mixing relationships for each. Thin solid lines in Figures 3a, 3e, and 3i are repeated in the panels below for comparison; in Figure 3l the thin line is obscured by the thick line. Horizontal lines in Figures 3a–3h indicate the snow–air interface (dashed) and the soil–snow interface (solid).

observed closer to one line or the other in Figure 2 depending on the dominant transport process. The isotopic effects of pressure pumping are illustrated in Figure 3. Profiles of CO_2 and $\delta^{13}C$ of CO_2 are shown during initially calm conditions just prior to a wind event (top panels), and 9, 18, and 48 h later. At the beginning the CO_2 profile varied from just over 3180 μmol mol^{-1} in the litter to 390 μmol mol^{-1} in the air above the snowpack (Figure 3a). This was associated with $\delta^{13}C$ of just under −22.0‰ in the litter and −8.3‰ in the air (Figure 3e). Mixing lines between $\delta^{13}C$ and CO_2 are shown in the right panels. Nine hours later, wind ventilation had decreased the gradient substantially, with CO_2 at 2100 μmol mol^{-1} in the litter, and a mid-snowpack minimum of 790 μmol mol^{-1}. The temporal difference in the CO_2 gradient is readily apparent in Figure 3b. This ventilation caused the mixing line to shift away from the original, in the advection-dominated direction (compare Figure 2a to Figures 3i and 3j). At 18 h, the CO_2 gradient was almost restored (Figure 3c), and the mixing line was moving back in the diffusion-only direction (Figure 3k). By 48 h the mixing line was indistinguishable from the original (Figure 3l; both lines are plotted).

[29] Snow depth reached a maximum of ~150 cm each winter, increasing during each storm and decreasing by settlement in the following days (Figure 4). Snow density generally increased over the winter and varied with height in the snowpack (Figure 4). The depth and mean density of hand-excavated pits compared favorably to continuous measurements of each at the SNOTEL site (Table 2), with significant linear regressions when pooled across winters. While there were vertical and horizontal differences in

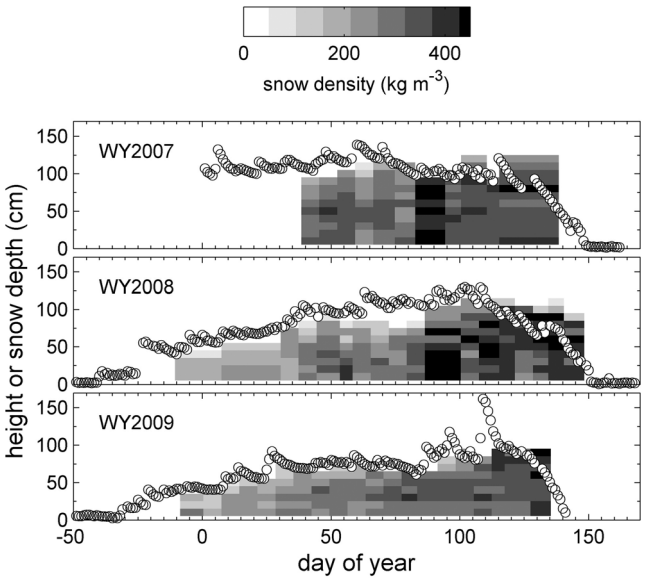

Figure 4. Snow depth at the SNOTEL site (open circles) and density profiles (from snow pits) during each winter (winter 1 on top, winter 3 on bottom). Density data are shown in 10 cm increments, and density is indicated by shading. Snow pit depth in the pits is indicated by the height of the density grid.

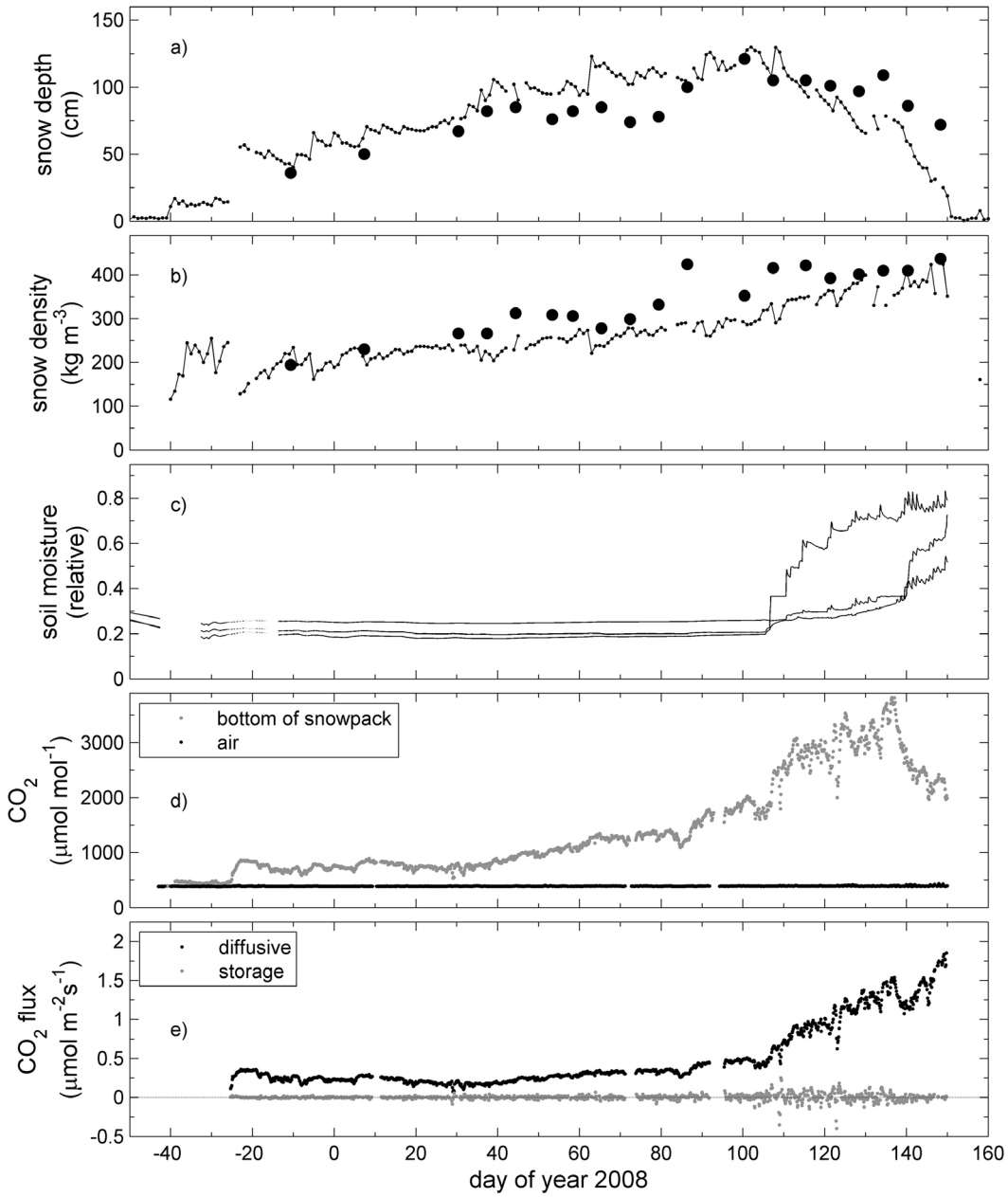

Figure 5. Biophysical parameters and CO_2 fluxes during winter 2 (2007/2008). (a) Snow depth and (b) bulk snow density at the SNOTEL site (dots with lines) and in hand-excavated pits (large circles), (c) soil moisture (0–10 cm depth), (d) CO_2 in the air and at the snow–soil interface, and (e) total regular CO_2 flux, with the diffusive ($^{12}F + {}^{13}F$) and storage ($^{12}F_s + {}^{13}F_s$) fluxes shown separately. These fluxes were calculated with the diffusion-only model. The enhancement to diffusive fluxes has not yet been applied; these are the measurements used to derive the enhanced diffusivity (equation (9)).

snowpack characteristics, these data provide some justification for using bulk physical parameters to calculate fluxes.

[30] Snow depth and density, soil moisture, CO_2, and CO_2 fluxes for W2 are shown in Figure 5. Melt events were generally restricted to late winter (Figure 5c; the melt pattern was similar for other winters). CO_2 in the air above the snowpack was near 390 μmol mol^{-1} for the entire winter but was higher at the bottom of the snowpack, increasing to ~4000 μmol mol^{-1} in late winter (Figure 5d). Diffusive CO_2 flux was less than 0.5 μmol m^{-2} s^{-1} until liquid water became available in late winter, then increased gradually to a peak near 2 μmol m^{-2} s^{-1} at end of melt (Figure 5e). The temporal pattern of the CO_2 mole fraction increase was different from that for the CO_2 flux increase, because the depth and density of the snowpack also changed (Figures 5a and 5b). Storage fluxes were very small compared to the diffusive fluxes (Figure 5e), reflecting the small amount of CO_2 stored in the snowpack relative to the flux moving through it.

[31] Data as shown in Figure 5 for all winters were used to examine the effect of wind on isotope mixing patterns. The

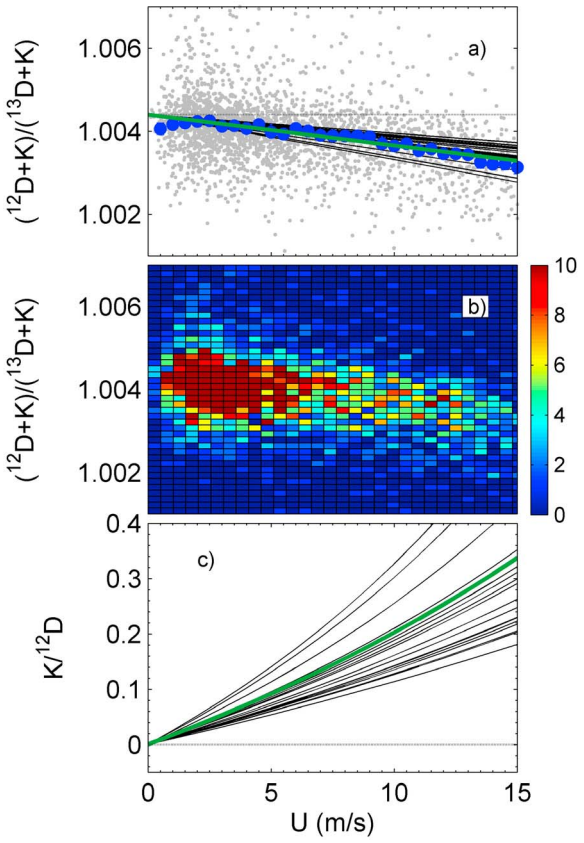

Figure 6. Dependence of the apparent isotopic fractionation associated with diffusion on above-canopy wind speed. When there is no wind ($U = 0$), the enhanced diffusivity (**K**) is zero, and the diffusivity ratio (equation (10)) converges to equation (3), with an intercept of 1.0044 (shown in Figure 6a as a horizontal dashed line). (a) Relationship between the diffusivity ratio and wind speed for all winters, including 3 h data (gray circles). Means (+/−1 SE error bars, smaller than symbols in some cases) are shown for wind bins of width 0.5 m s^{-1} (blue circles), and a linear regression (green solid line) through the 3 h data is shown (italicized in Table 3). Also shown (in black) are all the statistically significant regression lines from Tables 3 and 4. (b) Two-dimensional frequency distribution of the data in Figure 6a (color axis indicates number of occurrences). (c) The enhancement factor ($\mathbf{K}/^{12}D$) as a function of wind speed, which is derived via equation (10) from the regressions shown in Figure 6a. Quantities on the ordinate axes are dimensionless in all cases.

diffusivity ratio ($^{12}D + \mathbf{K}$)/($^{13}D + \mathbf{K}$) decreased with increasing above-canopy wind speed (Figure 6). There was scatter in the 3-hourly data (Figure 6a), but it was a highly statistically significant linear relationship. The pattern is easier to see when means and standard errors were plotted for narrow wind bins. Not all bins were equally represented in the data because the distribution of sampling varied with wind speed (Figure 6b). The slope of the linear relation in Figure 6a varied when calculated for winters individually or combined, or with different selections of inlets (Figure 6a and Table 3), and when snowpack depth and density were calculated using regressions of different types (Table 2). The three separate flux calculation methods used to examine W3 in detail also showed variability in the relation between ($^{12}D + \mathbf{K}$)/($^{13}D + \mathbf{K}$), and U (Figure 6a and Table 4). In all but two cases, highly significant linear relationships were obtained, with statistically significant slopes varying by a factor of 2 (-4.96 to -10.86×10^{-5}) (Tables 3 and 4 and Figure 6a) and always negative. The consistent negative slopes conform to our theoretical expectations of the isotopic effects of the wind enhancement of transport.

[32] The regression lines in Figure 6a were used to calculate the wind dependence of the enhancement factor $\mathbf{K}/^{12}D$ (Figure 6c). All significant regressions from Tables 3 and 4 are shown to illustrate the variability associated with method of calculation. We have highlighted the relation over all winters as the "best" estimate since it maximizes the use of observations and can be applied to all the years (Figures 6a and 6c (green lines) and Table 3 (italicized data)). Figure 6c can be interpreted as follows: depending on which line is chosen, a wind speed of 10 m s^{-1} leads to an enhancement of gas transport of 11%–33% higher than molecular diffusion alone ($\mathbf{K}/^{12}D$ = 0.11 to 0.33 at 10 m s^{-1}). For the best estimate the enhancement was 20% at 10 m s^{-1}.

[33] Recall that a wide range of values (−30‰ to −20‰) was assumed for the isotope ratio of soil respiration (δ_S), and the best regression for a set of conditions was chosen when it led to an intercept of 1.0044 in Figure 6a. The values of δ_S associated with the best regressions varied only minimally (−26.1‰ to −26.9‰) compared to the 10‰ range of values tested, indicating that the actual isotope ratio of soil respiration is probably in this narrow range.

[34] The distribution of the isotope ratios of the total fluxes over the three winters is shown in Figure 7. The mean isotope ratio of the total fluxes was −27.2‰ ± 1.1‰ (±1 SD), which was more negative than the assumed isotope ratios for δ_S that led to the best regressions between diffusivity ratio and U (from Tables 3 and 4), and to the measured bulk $\delta^{13}C$ of roots and soil in this forest (Figure 7b). The distribution had a larger tail in the more negative direction, with a skewness of −4.5 (dimensionless). Examination with respect to measured storage fluxes (Figure 8) revealed that the negative flux ratios were associated with negative storage fluxes (periods of CO_2 removal from the snowpack caused by wind ventilation; this will be explained later).

[35] The wind-dependent enhanced diffusivity from Figure 6 was used to calculate enhanced CO_2 fluxes, and time series of these quantities are shown in Figure 9. During this period the wind varied from 0 to 16 m s^{-1}, causing short-term enhancement of CO_2 transport 0%–36% higher than molecular diffusion alone ($K/^{12}D$ = 0 to 0.36) (Figure 9b). During the wind events, measured fluxes were lower because the gradient was decreased (Figure 9c), but for a given gradient the total transport was greater than from molecular diffusion. Periods of very low wind did not exhibit enhancement of transport (e.g., day 97, 6 April), but those with high winds showed strong enhancement (e.g., day 101, 10 April). Enhanced total fluxes for all three winters, and the cumulative fluxes for each winter are shown

Table 3. Summary of Results of Linear Regressions Between (^{12}D + **K**)/(^{13}D + **K**) (Where **K** is Calculated From Equation (10)) and Above-Canopy Wind Speed (21.5 m)[a]

Time Period	Slope (x10^{-5})	r^2	n	p	δ_s at 1.0044	Snow Regression Type	Inlets Used
All winters	−7.16	0.144	2711	<0.001	−26.6	Individual winters	0 and 200 cm
W1	−5.79	0.010	416	0.005 ns	−26.5	Individual winters	0 and 200 cm
W2	−5.48	0.152	1002	<0.001	−26.6	Individual winters	0 and 200 cm
W3	−5.84	0.240	426	<0.001	−26.6	Individual winters	0 and 200 cm
All winters	*−7.42*	*0.143*	*2811*	*<0.001*	*−26.6*	*Combined winters*	*0 and 200 cm*
W1	−6.63	0.030	608	<0.001	−26.6	Combined winters	0 and 200 cm
W2	−5.25	0.145	1118	<0.001	−26.6	Combined winters	0 and 200 cm
W3	−6.12	0.236	977	<0.001	−26.6	Combined winters	0 and 200 cm
All winters	−10.23	0.092	1448	<0.001	−26.2	Combined winters	60 and 200 cm
W1	−10.86	0.145	532	<0.001	−26.6	Combined winters	60 and 200 cm
W2	−5.50	0.086	625	<0.001	−26.1	Combined winters	60 and 200 cm
W3	+18.81	0.025	250	0.012 ns	−26.6	Combined winters	60 and 200 cm
W2 and W3	−6.77	0.103	1787	<0.001	−26.3	Combined winters	30 and 200 cm
W2	−8.97	0.150	1030	<0.001	−26.3	Combined winters	30 and 200 cm
W3	−4.51	0.064	749	<0.001	−26.3	Combined winters	30 and 200 cm

[a]Regressions were performed for the time periods of either the three winters separately or combined as indicated. Regression results were dependent on the assumed isotopic composition of the respiratory production source (δ_s). This value was varied from −30‰ to −20‰ in steps of 0.1‰, and for each value a regression between (^{12}D + **K**)/(^{13}D + **K**) and U was performed. Following this regression approach, the regression where the intercept equaled 1.0044 was selected, and the regression parameters (slope, r^2, n, p) and the value of δ_s where this occurred (δ_s at 1.0044) are shown. The probability of a significant correlation (p) was calculated with a t-test with n − 2 degrees of freedom (ns indicates a nonsignificant correlation). Snow depth, snow density, and air-filled porosity were calculated for use in Fick's law (equations (1) and (2)) using either data for all winters combined or each winter individually as indicated (as in Table 2, listed here as "Snow Regression Type"). All fluxes for Table 3 were calculated using flux method A. Inlets used for the flux calculations were located in the air (200 cm) and either at the bottom of the snowpack (0 cm) or within it (60 and 30 cm). No data were collected at the 30 cm inlet height during W1. The regression shown in italics was selected as the best regression and is highlighted in Figure 6.

in Figure 10 (enhanced fluxes were calculated using the green regression line in Figure 6).

5. Discussion

[36] This work provides direct evidence that pressure pumping enhances transport of CO_2 through a mountain forest seasonal snowpack, leading to total gas transport that is higher than by molecular diffusion alone. We used direct measurements of $^{12}CO_2$ and $^{13}CO_2$ mole fractions to demonstrate that pressure pumping alters trace gas transport via bulk airflow in the snowpack, so that the isotopic influence of diffusion is not always fully observed. Anecdotal events (such as those represented in Figure 3) suggest that CO_2 isotopic mixing patterns in snow are altered by wind over time scales of hours. The full analysis shows that advection is a persistent phenomenon when wind is present, and that the magnitude of the effect is wind dependent. In the absence of wind, diffusion dominates transport, the isotopic effects of diffusion dominate the observations, and the diffusivity ratio converges to 1.0044 as predicted by theory (Figure 6a and equations (3) and (10)). In the presence of wind, the diffusivity ratio is always less than 1.0044, again as predicted (negative slopes in Figure 6a). A variety of methods and assumptions were used to estimate the pressure pumping enhancement; these are shown as a family of lines in Figures 6a and 6c and listed in Tables 3 and 4. Regardless of the method used, the isotopic effect was consistent in sign (negative slopes in Figure 6a). Larger wind events were associated with larger isotopic effects.

[37] The relationship between diffusivity ratio and wind on a 3-hourly basis was statistically significant, but noisy. This is shown for a particular set of conditions in Figure 6a, but was generally true for all regressions examined. At least three factors contribute to this variability. First, the amount of CO_2 stored in the snowpack is small relative to the respiratory flux that moves through it, and to the large reservoir of CO_2 in the air. Transients associated with wind are likely to be more variable when a small reservoir is influenced on a time scale shorter than the time scale of wind disturbance. Second, the wind influence on trace gases is certainly not spatially or temporally uniform in the snowpack. Vertical and horizontal heterogeneity in snow depth, density, grain size and other physical attributes of the snowpack are well documented [*Colbeck*, 1991; *Dadic et al.*, 2008; *Molotch and Bales*, 2005] and were observed in our study (Figure 4). Pressure pumping likely influences bulk flow more near the top of the snowpack than the bottom [*Albert and Hawley*,

Table 4. Comparison of the Influence of Flux Method Used (A, B, or C) on the Regression Between (^{12}D + **K**)/(^{13}D + **K**) and U[a]

Flux Method	Slope (x10^{-5})	r^2	n	p	δ_s at 1.0044	Type
Method A	−5.84	0.240	426	<0.001	−26.6	With storage
Method B	−6.98	0.293	915	<0.001	−26.6	With storage
Method C	−7.66	0.213	917	<0.001	−26.6	With storage
Method A	−4.96	0.238	1036	<0.001	−26.8	Without storage
Method B	−5.01	0.291	915	<0.001	−26.8	Without storage
Method C	−5.36	0.198	919	<0.001	−26.9	Without storage

[a]Data are shown for winter 3 only. Details are as described in Table 3. Regressions were performed after calculating **K** using storage fluxes ("with storage," equation (9)) or assuming that storage fluxes were zero ("without storage").

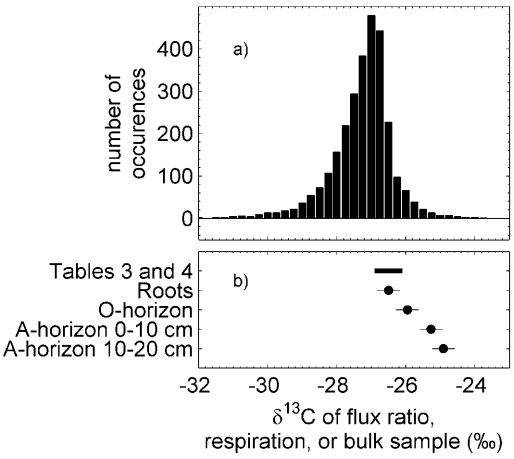

Figure 7. (a) Frequency distribution for the ratio of total fluxes $[(^{13}F + {}^{13}F_s)/(^{12}F + {}^{12}F_s)]$ converted to delta notation (equation (8)). Data for all winters are shown. (b) The range of values for the assumed isotope ratio of soil respiration (δ_s) that was associated with regression intercepts of 1.0044 (in Tables 3 and 4) and the measured δ^{13}C of bulk roots and soils [*Schaeffer et al.*, 2008] are shown for comparison.

2002; *Clifton et al.*, 2008]. Third, the diffusivity ratio was calculated using differences and ratios of sometimes small quantities (equations (9) and (10)), propagating analytical uncertainty and leading to high uncertainty on some values of **K**.

[38] The δ^{13}C of the flux ratio did not match that of respiration (δ_s associated with best fit regressions in Tables 3 and 4) nor that of bulk roots and soil (Figure 7). As we have shown elsewhere [*Bowling et al.*, 2009], the actual δ^{13}C of CO_2 in *air* within the snowpack is always bounded by the δ^{13}C of the two sources mixing (the air at −8 and respiratory CO_2 at perhaps −26‰ to −27‰ in our case) (Figure 2). In contrast to the air, the isotope ratio of the *fluxes* ($[(^{13}F + {}^{13}F_s)/(^{12}F + {}^{12}F_s)]$, in δ notation) was not always bounded by the sources (Figure 8). How can this unexpected result be explained? Isotope mixing under conditions of changing storage within the snowpack can be counterintuitive, as described for the atmosphere by *Miller and Tans* [2003]. Consider the flux from the snowpack at a given time to be a combination of a flux already within the snowpack (let this be F_a), and a flux from CO_2 added by a new source (F_b). Imagine initial conditions for the snowpack of a constant respiratory flux ($F_a = 1$ μmol m^{-2} s^{-1}) having a constant isotope ratio (δ_a = −26.6‰) (Figure 7). Further imagine that there has been a wind ventilation event and the gradient of CO_2 in the snowpack is smaller than it would be at steady state. If there is no subsequent wind, the gradient will increase over time as new flux F_b is added until it reaches a new steady state; this is a positive storage flux, represented in Figure 8 (right). This mixing can be described by a linear mixing model, where the isotope ratio of the total flux from the snowpack δ_s is given by [*Miller and Tans*, 2003] as

$$\delta_S = (\delta_a F_a + \delta_b F_b)/(F_a + F_b), \quad (14)$$

and δ_a and δ_b are the isotope ratio of the CO_2 in the snowpack and the added CO_2, respectively. If the flux of new CO_2 is added (F_b = 0 to +0.3 μmol m^{-2} s^{-1}) with the same isotope ratio as the flux that established the gradient in the first place ($\delta_a = \delta_b$ = −26.6‰), then there will be no change in the isotope ratio of the total flux from the snowpack (calculated with equation (14) and shown by the line in Figure 8 (right)). In contrast, if the initial conditions within the snowpack (F_a and δ_a as above) are changed by a removal of CO_2 caused by wind ventilation, the resulting flux will not always be between δ_a and δ_b. In this case, the flux added is air with δ_b = −8‰, and F_b = 0 to −0.3 μmol m^{-2} s^{-1} (negative indicating removal). This line is shown in Figure 8 (left). This theoretical perspective is consistent with the binned observations over the three winters of the study (Figure 8) and indicates that the actual isotope ratio of the respiration source is likely near −26.6‰. This is consistent with the values for respiration associated with the best regressions and the bulk values (Figure 7b).

[39] Our analysis is based on the assumption that the δ^{13}C of soil respiration under the snow (δ_s) is constant, and hence variation in isotopic mixing relationships is caused by to pressure pumping. Little is known about the δ_s in winter under the snow. Based on knowledge from a recent literature review [*Bowling et al.*, 2008], in an earlier study at the Niwot Ridge forest [*Bowling et al.*, 2009] we expected to find variability in δ_s, particularly associated with two events. First, the initial appearance of liquid water from melting snow would be expected to enhance microbial activity. The soil under the snow in winter is usually below field capacity, and soil moisture is highly dependent on conditions in the fall before the snowpack develops. Added moisture probably enhances the activity of the subnivean fungal community [*Schmidt et al.*, 2009] and leads to the higher CO_2 fluxes observed in late winter (Figure 5e and Figure 10a). Second, initiation of transpiration and net carbon uptake by the Niwot Ridge forest occurs in winter long before the snowpack is gone [*Monson et al.*, 2005]. Neither of these

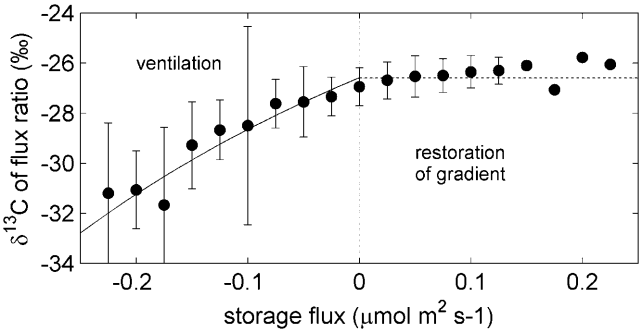

Figure 8. The influence of the storage flux on the δ^{13}C of the flux ratio (as in Figure 7a). Means (+/−1 SD error bars) are shown for storage flux bins of width 0.025 μmol m^2 s^{-1} (missing error bars indicate fewer than 3 samples). The right half of the figure (positive storage flux) represents periods when the CO_2 stored in the snowpack increased as respiratory CO_2 was added during calm conditions. The left half represents a decrease in the CO_2 stored as the snowpack was ventilated by wind. The lines were calculated using equation (14) as described in the text.

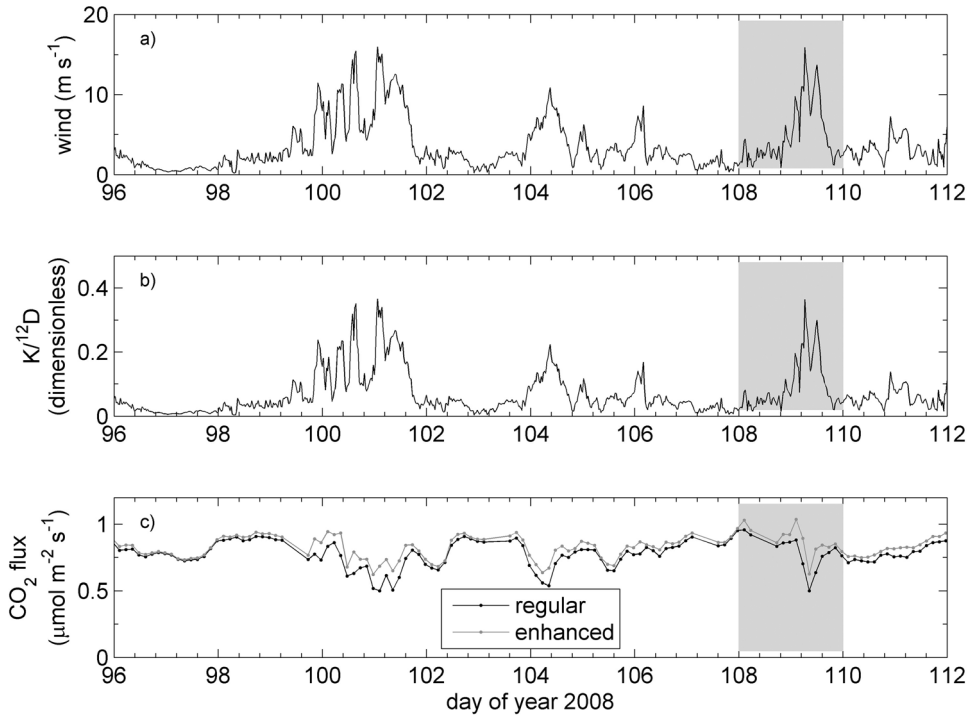

Figure 9. Sixteen-day time series of (a) above-canopy wind speed, (b) enhancement factor ($\mathbf{K}/^{12}$D), calculated from the wind velocity regression for all winters (method A, shown in Figure 6), and (c) total CO_2 flux calculated with and without the enhancement to diffusion. The enhanced fluxes ($^{12}F_{enh} + {}^{12}F_s + {}^{13}F_{enh} + {}^{13}F_s$) are shown in gray, and the regular fluxes ($^{12}F + {}^{12}F_s + {}^{13}F + {}^{13}F_s$) are shown in black. The time period detailed in Figure 3 is highlighted in the gray box.

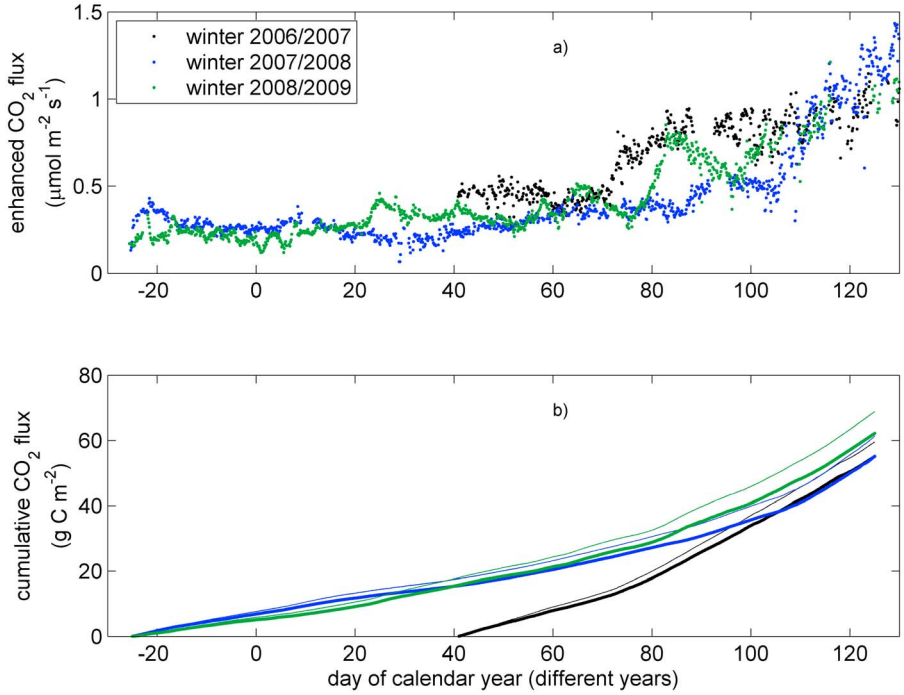

Figure 10. (a) Comparison of total cumulative CO_2 flux over the three winters of the study. (b) Cumulative CO_2 flux during each winter, shown with enhancement (thin lines) and without enhancement (thick lines) of transport caused by pressure pumping. Enhancement was calculated using the best regression (shown in Figure 6 as a green line). The time periods when fluxes were summed differed during the winters due to differences in initiation of measurement (e.g., measurements during W1 began on the 41st day of the year). Fluxes in both panels were calculated including storage as described for Figure 9.

events led to a change in δ_s that was detectable beyond the variability induced by wind [*Bowling et al.*, 2009]. If δ_s varied for biological reasons in the present study, it would certainly complicate our results. However, the generality of the relationships shown in Figure 6a provides confidence that the isotopic variability was primarily caused by wind.

[40] The degree of enhancement of transport varied with flux method (Figure 6c), and the magnitude of cumulative enhancement over each winter differed (Figure 10b). This variation allows us to put some bounds on the most likely magnitude of the pressure pumping effect. The regular fluxes summed to 55.1, 55.6, and 62.2 g C m^{-2} per time interval during winters 1, 2, and 3, respectively; and the enhanced fluxes, calculated using the green line in Figures 6a and 6c, were 60.0, 61.3, and 68.8 g C m^{-2} (Figure 10b). These winter carbon fluxes are significant when compared to the annual net ecosystem productivity of this forest, which varies from 20 to 100 g C m^{-2} yr^{-1} [*Hu et al.*, 2010]. These values represent a mean enhancement of transport caused by pressure pumping over each winter of 8.9, 11.0, and 11.1% (percent) beyond molecular diffusion. Enhanced cumulative fluxes were also calculated for W3 using the significant regressions from Tables 3 and 4. These are not shown in Figure 10, but the values ranged from 65.9 to 72.8 g C m^{-2}, corresponding to variability in the mean enhancement of transport estimated from the different methods of 1.1% to 11.7% for W3. Hence, pressure pumping in our forest snowpack can enhance transport beyond molecular diffusion by up to 40% in the short term (Figure 9), but by at most around 11% when accumulated over a winter. This is smaller than the spatial variability of under snow respiration within similar nearby subalpine forests (<30 km away), which showed a coefficient of variation of 29% [*Hubbard et al.*, 2005]. However, the effect is persistent and will systematically increase fluxes across the landscape relative to the diffusive rate.

[41] Several groups have shown that CO_2 within the snowpack is related to wind velocity or pressure [e.g., *Jones et al.*, 1999; *Suzuki et al.*, 2006; *Takagi et al.*, 2005], but to our knowledge only *Seok et al.* [2009] have attempted to quantify the magnitude of the pressure pumping effect on transport. These researchers used regressions of CO_2 mole fraction at various depths versus wind velocity to extrapolate to an idealized profile under no-wind conditions. They then applied Fick's first law to the extrapolated CO_2 profile to calculate the expected flux if there was no wind. Seok and colleagues found that under conditions of no wind, fluxes would be 56% higher than observed under actual conditions assuming diffusive transport. This implies that by reducing the mole fraction gradients, wind reduces the short-term flux, in agreement with our results (Figure 9c). However, as we have shown, the persistent but subtle influence of wind on bulk flow within the snowpack actually *increases* the flux beyond the molecular diffusion transport rate. We attempted to use their regression method for comparison to their results, but our regressions of CO_2 versus wind were extremely noisy and did not provide confident estimation of profiles under calm conditions.

[42] A few caveats in our analysis should be noted. First, we have neglected the physical complexity of the layering of the snowpack. Gradients of snow density within the pack (Figure 3) and variations in grain size and type will influence transport, and the total transport may or may not be accurately captured by using bulk snowpack physical parameters. This is particularly true if ice layers develop during rain-on-snow events, or melt-freeze events caused by sun or warm cloudy conditions. Such layers may limit the pressure pumping influence to the snow above the ice layer, and may lead to kinks in trace gas profiles [*Jones et al.*, 1999]. Second, the influence of wind direction on the pressure fields within the snowpack may be important, particularly in the presence of local terrain features [*Staebler and Fitzjarrald*, 2005] or snow surface roughness [*Albert*, 2002]. Third, we have ignored the process of CO_2 dissolution in water via the carbonic acid reactions. While this is probably unimportant in the cold dry winter snowpack, during melt the water in the snowpack and in the soil may be an important reservoir for dissolved CO_2 [*Flechard et al.*, 2007; *Gamnitzer et al.*, 2011]. Finally, additional physical fractionation mechanisms such as thermal diffusion, gravitational settling, or water vapor diffusion may contribute [*Severinghaus et al.*, 1996], but their effects are likely to be small.

[43] These results are applicable to biogeochemical systems beyond the snowpack. This study and others [e.g., *Seok et al.*, 2009; *Takagi et al.*, 2005] have demonstrated that pressure pumping can dramatically alter trace gas mole fractions in the soil even when covered with a snowpack 1–2 m deep (Figure 3). By extension, one should expect that pressure pumping influences gas transport in soils year-round, and the effect is potentially larger when the soils are snow-free because the pressure field is not dampened by snow. Wind effects on soil gases, some penetrating to many decimeters, have been reported in moss organic horizons of boreal forests [*Hirsch et al.*, 2004], in crop soils [*Reicosky et al.*, 2008], those of a temperate grassland [*Flechard et al.*, 2007], a Scots pine forest [*Maier et al.*, 2010], an urban temperate deciduous stand [*Fujiyoshi et al.*, 2010], and soils subjected to volcanic outgassing [*Viveiros et al.*, 2009]. Experimental studies with CO_2 leakage from geologic storage sites have identified the importance of nondiffusive transport [*Amonette et al.*, 2010; *Lewicki et al.*, 2010], and it can be a factor influencing radon emission [*Fujiyoshi et al.*, 2010], contaminant transport [*Auer et al.*, 1996], and geochemical redox processes [*Elberling et al.*, 1998].

6. Conclusions

[44] In this study, we have developed theory and methods to use stable isotopes of CO_2 to investigate the relative contributions of diffusion and advection in trace gas transport. Pressure pumping was a persistent feature of transport in this mountain forest seasonal snowpack, causing short-term enhancement up to 40% higher than molecular diffusion, but 11% over a winter. It is highly likely that pressure pumping influences soil gas transport in general, and future research should investigate the importance of this process in soils.

[45] **Acknowledgments.** CO_2 isotope data from the Niwot Ridge AmeriFlux site, including the undersnow data, are available for collaborative use by any interested researcher; contact the corresponding author. D. R. B. is grateful to the U.S. Forest Service Rocky Mountain Research Station for hosting a sabbatical visit. Thanks to Sean Burns and Russ Monson for sharing wind data, to John Knowles and Kurt Chowanski for outstanding field assistance, and to Thure Cerling, Greg Maurer, and Mark Williams for helpful discussions. We are grateful for logistical support from

the Niwot Ridge Long-Term Ecological Research Program, funded by the National Science Foundation (NSF). Thanks to the U.S. Department of Agriculture Natural Resources Conservation Service, Colorado Snow Survey Program, for maintaining the SNOTEL network and sharing their data. This research was supported by the Office of Science (BER), U.S. Department of Energy, grant DE-FG02-04ER63904, and NSF grant DEB 0743251.

References

Albert, M. R. (2002), Effects of snow and firn ventilation on sublimation rates, *Ann. Glaciol.*, *35*, 52–56, doi:10.3189/172756402781817194.

Albert, M. R., and J. P. Hardy (1995), Ventilation experiments in a seasonal snow cover, in *Biogeochemistry of Seasonally Snow-Covered Catchments*, edited by K. A. Tonnessen, M. A. Williams, and M. Tranter, pp. 41–49, Int. Assoc. of Hydrol. Sci. Press, Inst. of Hydrol., Wallingford, U. K.

Albert, M. R., and R. L. Hawley (2002), Seasonal changes in snow surface roughness characteristics at Summit, Greenland: Implications for snow and firn ventilation, *Ann. Glaciol.*, *35*, 510–514, doi:10.3189/172756402781816591.

Albert, M. R., and E. F. Shultz (2002), Snow and firn properties and air-snow transport processes at Summit, Greenland, *Atmos. Environ.*, *36*, 2789–2797, doi:10.1016/S1352-2310(02)00119-X.

Amonette, J. E., J. L. Barr, L. M. Dobeck, K. Gullickson, and S. J. Walsh (2010), Spatiotemporal changes in CO_2 emissions during the second ZERT injection, August–September 2008, *Environ. Earth Sci.*, *60*, 263–272, doi:10.1007/s12665-009-0402-0.

Auer, L. H., N. D. Rosenberg, K. H. Birdsell, and E. M. Whitney (1996), The effects of barometric pumping on contaminant transport, *J. Contam. Hydrol.*, *24*, 145–166, doi:10.1016/S0169-7722(96)00010-1.

Björkman, M. P., E. Morgner, E. J. Cooper, B. Elberling, L. Klemedtsson, and R. G. Björk (2010), Winter carbon dioxide effluxes from Arctic ecosystems: An overview and comparison of methodologies, *Global Biogeochem. Cycles*, *24*, GB3010, doi:10.1029/2009GB003667.

Bottacin-Busolin, A., and A. Marion (2010), Combined role of advective pumping and mechanical dispersion on time scales of bed form–induced hyporheic exchange, *Water Resour. Res.*, *46*, W08518, doi:10.1029/2009WR008892.

Bowling, D. R., D. E. Pataki, and J. T. Randerson (2008), Carbon isotopes in terrestrial ecosystem pools and CO_2 fluxes, *New Phytol.*, *178*, 24–40, doi:10.1111/j.1469-8137.2007.02342.x.

Bowling, D. R., W. J. Massman, S. M. Schaeffer, S. P. Burns, R. K. Monson, and M. W. Williams (2009), Biological and physical influences on the carbon isotope content of CO_2 in a subalpine forest snowpack, Niwot Ridge, Colorado, *Biogeochemistry*, *95*, 37–59, doi:10.1007/s10533-008-9233-4.

Camarda, M., S. De Gregorio, R. Favara, and S. Gurrieri (2007), Evaluation of carbon isotope fractionation of soil CO_2 under an advective–diffusive regimen: A tool for computing the isotopic composition of unfractionated deep source, *Geochim. Cosmochim. Acta*, *71*(12), 3016–3027, doi:10.1016/j.gca.2007.04.002.

Cerling, T. E., D. K. Solomon, J. Quade, and J. R. Bowman (1991), On the isotopic composition of carbon in soil carbon dioxide, *Geochim. Cosmochim. Acta*, *55*(11), 3403–3405, doi:10.1016/0016-7037(91)90498-T.

Clarke, G. K. C., and E. D. Waddington (1991), A three-dimensional theory of wind pumping, *J. Glaciol.*, *37*, 89–96.

Clifton, A., C. Manes, J. D. Ruedi, M. Guala, and M. Lehning (2008), On shear-driven ventilation of snow, *Boundary Layer Meteorol.*, *126*, 249–261, doi:10.1007/s10546-007-9235-0.

Colbeck, S. C. (1989), Air movement in snow due to windpumping, *J. Glaciol.*, *35*, 209–213.

Colbeck, S. C. (1991), The layered character of snow covers, *Rev. Geophys.*, *29*(1), 81–96, doi:10.1029/90RG02351.

Dadic, R., M. Schneebeli, M. Lehning, M. A. Hutterli, and A. Ohmura (2008), Impact of the microstructure of snow on its temperature: A model validation with measurements from Summit, Greenland, *J. Geophys. Res.*, *113*, D14303, doi:10.1029/2007JD009562.

Elberling, B., and K. K. Brandt (2003), Uncoupling of microbial CO_2 production and release in frozen soil and its implications for field studies of arctic C cycling, *Soil Biol. Biochem.*, *35*, 263–272, doi:10.1016/S0038-0717(02)00258-4.

Elberling, B., F. Larsen, S. Christensen, and D. Postma (1998), Gas transport in a confined unsaturated zone during atmospheric pressure cycles, *Water Resour. Res.*, *34*, 2855–2862, doi:10.1029/98WR02037.

Flechard, C. R., A. Neftel, M. Jocher, C. Ammann, J. Leifeld, and J. Fuhrer (2007), Temporal changes in soil pore space CO_2 concentration and storage under permanent grassland, *Agric. For. Meteorol.*, *142*, 66–84, doi:10.1016/j.agrformet.2006.11.006.

Fujiyoshi, R., Y. Haraki, T. Sumiyoshi, H. Amano, I. Kobal, and J. Vaupotič (2010), Tracing the sources of gaseous components (^{222}Rn, CO_2 and its carbon isotopes) in soil air under a cool-deciduous stand in Sapporo, Japan, *Environ. Geochem. Health*, *32*, 73–82, doi:10.1007/s10653-009-9266-1.

Gamnitzer, U., A. B. Moyes, D. R. Bowling, and H. Schnyder (2011), Measuring and modeling the isotopic composition of soil respiration: Insights from a grassland tracer experiment, *Biogeosciences*, *8*, 1333–1350, doi:10.5194/bg-8-1333-2011.

Groffman, P. M., J. P. Hardy, C. T. Driscoll, and T. J. Fahey (2006), Snow depth, soil freezing, and fluxes of carbon dioxide, nitrous oxide and methane in a northern hardwood forest, *Global Change Biol.*, *12*, 1748–1760, doi:10.1111/j.1365-2486.2006.01194.x.

Helmig, D., E. Apel, D. Blake, L. Ganzeveld, B. L. Lefer, S. Meinardi, and A. L. Swanson (2009), Release and uptake of volatile inorganic and organic gases through the snowpack at Niwot Ridge, Colorado, *Biogeochemistry*, *95*, 167–183, doi:10.1007/s10533-009-9326-8.

Hirsch, A. I., S. E. Trumbore, and M. L. Goulden (2004), The surface CO_2 gradient and pore-space storage flux in a high-porosity litter layer, *Tellus, Ser. B*, *56*, 312–321.

Honrath, R. E., Y. Lu, M. C. Peterson, J. E. Dibb, M. A. Arsenault, N. J. Cullen, and K. Steffen (2002), Vertical fluxes of NO_x, HONO, and HNO_3 above the snowpack at Summit, Greenland, *Atmos. Environ.*, *36*, 2629–2640, doi:10.1016/S1352-2310(02)00132-2.

Hu, J., D. J. P. Moore, S. P. Burns, and R. K. Monson (2010), Longer growing seasons lead to less carbon sequestration by a subalpine forest, *Global Change Biol.*, *16*, 771–783, doi:10.1111/j.1365-2486.2009.01967.x.

Hubbard, R. M., M. G. Ryan, K. Elder, and C. C. Rhoades (2005), Seasonal patterns in soil surface CO_2 flux under snow cover in 50 and 300 year old subalpine forests, *Biogeochemistry*, *73*, 93–107, doi:10.1007/s10533-004-1990-0.

Jones, H. G., J. W. Pomeroy, T. D. Davies, M. Tranter, and P. Marsh (1999), CO_2 in Arctic snow cover: Landscape form, in-pack gas concentration gradients, and the implications for the estimation of gaseous fluxes, *Hydrol. Processes*, *13*, 2977–2989, doi:10.1002/(SICI)1099-1085(19991230)13:18<2977::AID-HYP12>3.0.CO;2-#.

Kawamura, K., J. P. Severinghaus, S. Ishidoya, S. Sugawara, G. Hashida, H. Motoyama, Y. Fujii, S. Aoki, and T. Nakazawa (2006), Convective mixing of air in firn at four polar sites, *Earth Planet. Sci. Lett.*, *244*, 672–682, doi:10.1016/j.epsl.2006.02.017.

Keeling, C. D. (1958), The concentration and isotopic abundances of atmospheric carbon dioxide in rural areas, *Geochim. Cosmochim. Acta*, *13*(4), 322–334, doi:10.1016/0016-7037(58)90033-4.

Kelley, J. J., D. F. Weaver, and B. P. Smith (1968), The variation of carbon dioxide under the snow in the Arctic, *Ecology*, *49*, 358–361, doi:10.2307/1934472.

Kimball, B. A., and E. R. Lemon (1970), Spectra of air pressure fluctuations at the soil surface, *J. Geophys. Res.*, *75*(33), 6771–6777, doi:10.1029/JC075i033p06771.

Kimball, B. A., and E. R. Lemon (1971a), Air turbulence effects upon soil gas exchange, *Soil Sci. Soc. Am. J.*, *35*, 16–21, doi:10.2136/sssaj1971.03615995003500010013x.

Kimball, B. A., and E. R. Lemon (1971b), Theory of soil air movement due to pressure fluctuations, *Agric. Meteorol.*, *9*, 163–181, doi:10.1016/0002-1571(71)90020-3.

Lafleur, P. M., N. T. Roulet, and S. W. Admiral (2001), Annual cycle of CO_2 exchange at a bog peatland, *J. Geophys. Res.*, *106*(D3), 3071–3081, doi:10.1029/2000JD900588.

Lewicki, J. L., G. E. Hilley, L. Dobeck, and L. Spangler (2010), Dynamics of CO_2 fluxes and concentrations during a shallow subsurface CO_2 release, *Environ. Earth Sci.*, *60*, 285–297, doi:10.1007/s12665-009-0396-7.

Liptzin, D., M. W. Williams, D. Helmig, B. Seok, G. Filippa, K. Chowanski, and J. Hueber (2009), Process-level controls on CO_2 fluxes from a seasonally snow-covered subalpine meadow soil, Niwot Ridge, Colorado, *Biogeochemistry*, *95*, 151–166, doi:10.1007/s10533-009-9303-2.

Maier, M., H. Schack-Kirchner, E. E. Hildebrand, and J. Holst (2010), Pore-space CO_2 dynamics in a deep, well-aerated soil, *Eur. J. Soil Sci.*, *61*, 877–887, doi:10.1111/j.1365-2389.2010.01287.x.

Massman, W. J. (1998), A review of the molecular diffusivities of H_2O, CO_2, CH_4, CO, O_3, SO_2, NH_3, N_2O, NO, and NO_2 in air, O_2 and N_2 near STP, *Atmos. Environ.*, *32*, 1111–1127, doi:10.1016/S1352-2310(97)00391-9.

Massman, W. J. (2006), Advective transport of CO_2 in permeable media induced by atmospheric pressure fluctuations: 1. An analytical model, *J. Geophys. Res.*, *111*, G03004, doi:10.1029/2006JG000163.

Massman, W. J., and J. M. Frank (2006), Advective transport of CO_2 in permeable media induced by atmospheric pressure fluctuations: 2. Observational evidence under snowpacks, *J. Geophys. Res.*, *111*, G03005, doi:10.1029/2006JG000164.

Massman, W. J., R. A. Sommerfeld, A. R. Mosier, K. F. Zeller, T. J. Hehn, and S. G. Rochelle (1997), A model investigation of turbulence-driven pressure-pumping effects on the rate of diffusion of CO_2, N_2O, and CH_4

through layered snowpacks, *J. Geophys. Res.*, *102*(D15), 18,851–18,863, doi:10.1029/97JD00844.

Mastepanov, M., C. Sigsgaard, E. J. Dlugokencky, S. Houweling, L. Strom, M. P. Tamstorf, and T. R. Christensen (2008), Large tundra methane burst during onset of freezing, *Nature*, *456*, 628–630, doi:10.1038/nature07464.

McDowell, N. G., J. D. Marshall, T. D. Hooker, and R. Musselman (2000), Estimating CO_2 flux from snowpacks at three sites in the Rocky Mountains, *Tree Physiol.*, *20*, 745–753, doi:10.1093/treephys/20.11.745.

Miller, J. B., and P. P. Tans (2003), Calculating isotopic fractionation from atmospheric measurements at various scales, *Tellus, Ser. B*, *55*, 207–214, doi:10.1034/j.1600-0889.2003.00020.x.

Molotch, N. P., and R. C. Bales (2005), Scaling snow observations from the point to the grid element: Implications for observation network design, *Water Resour. Res.*, *41*, W11421, doi:10.1029/2005WR004229.

Monson, R. K., A. A. Turnipseed, J. P. Sparks, P. C. Harley, L. E. Scott-Denton, K. Sparks, and T. E. Huxman (2002), Carbon sequestration in a high-elevation, subalpine forest, *Global Change Biol.*, *8*, 459–478, doi:10.1046/j.1365-2486.2002.00480.x.

Monson, R. K., J. P. Sparks, T. N. Rosenstiel, L. E. Scott-Denton, T. E. Huxman, P. C. Harley, A. A. Turnipseed, S. P. Burns, B. Backlund, and J. Hu (2005), Climatic influences on net ecosystem CO_2 exchange during the transition from wintertime carbon source to springtime carbon sink in a high-elevation, subalpine forest, *Oecologia*, *146*, 130–147, doi:10.1007/s00442-005-0169-2.

Monson, R. K., S. P. Burns, M. W. Williams, A. C. Delany, M. Weintraub, and D. A. Lipson (2006), The contribution of beneath-snow soil respiration to total ecosystem respiration in a high-elevation, subalpine forest, *Global Biogeochem. Cycles*, *20*, GB3030, doi:10.1029/2005GB002684.

Pataki, D. E., J. R. Ehleringer, L. B. Flanagan, D. Yakir, D. R. Bowling, C. J. Still, N. Buchmann, J. O. Kaplan, and J. A. Berry (2003), The application and interpretation of Keeling plots in terrestrial carbon cycle research, *Global Biogeochem. Cycles*, *17*(1), 1022, doi:10.1029/2001GB001850.

Reicosky, D. C., R. W. Gesch, S. W. Wagner, R. A. Gilbert, C. D. Wente, and D. R. Morris (2008), Tillage and wind effects on soil CO_2 concentrations in muck soils, *Soil Tillage Res.*, *99*, 221–231, doi:10.1016/j.still.2008.02.006.

Schaeffer, S. M., D. E. Anderson, S. P. Burns, R. K. Monson, J. Sun, and D. R. Bowling (2008), Canopy structure and atmospheric flows in relation to the $\delta^{13}C$ of respired CO_2 in a subalpine coniferous forest, *Agric. For. Meteorol.*, *148*, 592–605, doi:10.1016/j.agrformet.2007.11.003.

Schmidt, S. K., K. L. Wilson, R. K. Monson, and D. A. Lipson (2009), Exponential growth of "snow molds" at sub-zero temperatures: An explanation for high beneath-snow respiration rates and Q_{10} values, *Biogeochemistry*, *95*, 13–21, doi:10.1007/s10533-008-9247-y.

Scott-Denton, L. E., K. L. Sparks, and R. K. Monson (2003), Spatial and temporal controls of soil respiration rate in a high-elevation, subalpine forest, *Soil Biol. Biochem.*, *35*, 525–534, doi:10.1016/S0038-0717(03)00007-5.

Seok, B., D. Helmig, M. W. Williams, D. Liptzin, K. Chowanski, and J. Hueber (2009), An automated system for continuous measurements of trace gas fluxes through snow: An evaluation of the gas diffusion method at a subalpine forest site, Niwot Ridge, Colorado, *Biogeochemistry*, *95*, 95–113, doi:10.1007/s10533-009-9302-3.

Severinghaus, J. P., M. L. Bender, R. F. Keeling, and W. S. Broecker (1996), Fractionation of soil gases by diffusion of water vapor, gravitational settling, and thermal diffusion, *Geochim. Cosmochim. Acta*, *60*(6), 1005–1018, doi:10.1016/0016-7037(96)00011-7.

Sokratov, S. A., and A. Sato (2000), Wind propagation to snow observed in laboratory, *Ann. Glaciol.*, *31*, 427–433, doi:10.3189/172756400781820020.

Sommerfeld, R. A., A. R. Mosier, and R. C. Musselman (1993), CO_2, CH_4 and N_2O flux through a Wyoming snowpack and implications for global budgets, *Nature*, *361*, 140–142, doi:10.1038/361140a0.

Sommerfeld, R. A., W. J. Massman, R. C. Musselman, and A. R. Mosier (1996), Diffusional flux of CO_2 through snow: Spatial and temporal variability among alpine-subalpine sites, *Global Biogeochem. Cycles*, *10*(3), 473–482, doi:10.1029/96GB01610.

Staebler, R. M., and D. R. Fitzjarrald (2005), Measuring canopy structure and the kinematics of subcanopy flows in two forests, *J. Appl. Meteorol.*, *44*, 1161–1179, doi:10.1175/JAM2265.1.

Sturm, M., and J. B. Johnson (1991), Natural convection in the subarctic snow cover, *J. Geophys. Res.*, *96*(B7), 11,657–11,671, doi:10.1029/91JB00895.

Suzuki, S., S. Ishizuka, K. Kitamura, K. Yamanoi, and Y. Nakai (2006), Continuous estimation of winter carbon dioxide efflux from the snow surface in a deciduous broadleaf forest, *J. Geophys. Res.*, *111*, D17101, doi:10.1029/2005JD006595.

Takagi, K., M. Nomura, D. Ashiya, H. Takahashi, K. Sasa, Y. Fujinuma, H. Shibata, Y. Akibayashi, and T. Koike (2005), Dynamic carbon dioxide exchange through snowpack by wind-driven mass transfer in a conifer-broadleaf mixed forest in northernmost Japan, *Global Biogeochem. Cycles*, *19*, GB2012, doi:10.1029/2004GB002272.

Turnipseed, A. A., P. D. Blanken, D. E. Anderson, and R. K. Monson (2002), Energy budget above a high-elevation subalpine forest in complex topography, *Agric. For. Meteorol.*, *110*, 177–201, doi:10.1016/S0168-1923(01)00290-8.

Viveiros, F., T. Ferreira, C. Silva, and J. L. Gaspar (2009), Meteorological factors controlling soil gases and indoor CO_2 concentration: A permanent risk in degassing areas, *Sci. Total Environ.*, *407*, 1362–1372, doi:10.1016/j.scitotenv.2008.10.009.

Waddington, E. D., J. Cunningham, and S. L. Harder (1996), The effects of snow ventilation on chemical concentrations, in *Chemical Exchange Between the Atmosphere and Polar Snow*, edited by E. W. Wolff and R. C. Bales, pp. 403–451, Springer, Berlin.

Williams, M. W., D. Cline, M. Hartman, and T. Bardsley (1999), Data for snowmelt model development, calibration, and verification at an alpine site, Colorado Front Range, *Water Resour. Res.*, *35*, 3205–3209, doi:10.1029/1999WR900088.

Wu, X., N. Brüggemann, R. Gasche, Z. Shen, B. Wolf, and K. Butterbach-Bahl (2010), Environmental controls over soil-atmosphere exchange of N_2O, NO, and CO_2 in a temperate Norway spruce forest, *Global Biogeochem. Cycles*, *24*, GB2012, doi:10.1029/2009GB003616.

D. R. Bowling, Department of Biology, University of Utah, 257 South 1400 East, Salt Lake City, UT 84112-0820, USA. (david.bowling@utah.edu)

W. J. Massman, USDA Forest Service, 240 West Prospect Rd., Fort Collins, CO 80526, USA.